

1 **Untangling irrigation effects on maize water and heat stress** 2 **alleviation using satellite data**

3
4 Peng Zhu^{1*}, Jennifer Burney¹

5 ¹School of Global Policy and Strategy, University of California, San Diego, CA USA

6 *Correspondence to:* Peng Zhu (zhuyp678@gmail.com)

7
8 **Abstract.** Irrigation has important implications for sustaining global food production,
9 enabling crop water demand to be met even under dry conditions. Added water also
10 cools crop plants through transpiration; irrigation might thus play an important role in
11 a warmer climate by simultaneously moderating water and high temperature stresses.
12 Here we used satellite-derived evapotranspiration estimates, land surface temperature
13 (LST) measurements, and crop phenological stage information from Nebraska maize
14 to quantify how irrigation relieves both water and temperature stresses. Unlike air
15 temperature metrics, satellite-derived LST revealed a significant irrigation-induced
16 cooling effect, especially during the grain filling period (GFP) of crop growth. This
17 cooling appeared to extend the maize growing season, especially for GFP, likely due
18 to the stronger temperature sensitivity of phenological development during this stage.
19 Our analysis also revealed that irrigation not only reduced water and temperature
20 stress but also weakened the response of yield to these stresses. Specifically,
21 temperature stress was significantly weakened for reproductive processes in irrigated
22 maize. Attribution analysis further suggested that water and high temperature stress
23 alleviation were responsible for $65\pm 10\%$ and $35\pm 5.3\%$ of irrigation's yield benefit,
24 respectively. Our study underlines the relative importance of high temperature stress
25 alleviation in yield improvement and the necessity of simulating crop surface
26 temperature to better quantify heat stress effects in crop yield models. Finally,
27 considering the potentially strong interaction between water and heat stress, future
28 research on irrigation benefits should explore the interaction effects between heat and
29 drought alleviation.

30
31 **Keywords:** Irrigation, Evaporative cooling, MODIS LST, High temperature
32 stress, Water stress, Maize

34 **1. Introduction**

35 Irrigation -- a large component of freshwater consumption sourced from water
36 diversion from streams and groundwater (Wallace, 2000, Howell, 2001) -- allows
37 crops to grow in environments that do not receive sufficient rainfall, and buffers
38 agricultural production from climate variability and extremes. Irrigated agriculture
39 plays an outsized role in global crop production and food security: irrigated lands
40 account for 17% of total cropped area, yet they provide 40% of global cereals
41 (Rosegrant et al 2002, Siebert and Döll 2010). Meeting the rising food demands of a
42 growing global population will require either increasing crop productivity and/or
43 expansion of cropped areas; both strategies are daunting under projected climate
44 change. Cropland expansion may be in marginal areas that require irrigation even in
45 the present climate (Bruinsma 2009); increasing temperatures will drive higher
46 atmospheric vapor pressure deficits (VPD) and raise crop water demand and crop
47 water losses. This increasing water demand poses a water ceiling for crop growth and
48 might necessitate irrigation application over present rainfed areas to increase or even
49 maintain yields (DeLucia et al., 2019).

50

51 However, the provision of additional irrigation water modifies both the land surface
52 water and energy budgets. Additional water can result in an evaporative cooling
53 effect, which may be beneficial for crop growth indirectly through lowering the
54 frequency of extreme heat stress (Butler et al., 2018). High temperature stress will be
55 more prevalent (Russo et al., 2014) under future warming, and might result in more
56 severe yield losses than water stress (Zhu et al., 2019) due to reduced photosynthesis,
57 pollen sterility, and accelerated crop senescence in major cereals (Rezaei et al.,
58 2015b; Rattalino Edreira et al., 2011; Ruiz-Vera et al., 2018). A better understanding
59 of irrigation's potential to alleviate high temperature stress will therefore be important
60 for agricultural management. More broadly, understanding how irrigation can or
61 should contribute to a portfolio of agricultural adaptation strategies thus requires
62 improved understanding of its relative roles in mitigating both water and heat stresses.

63

64 Climate models and meteorological data have been used to investigate how historical
65 expansion of irrigation at global and regional scales has influenced the climate
66 system, including surface cooling and precipitation variation (Kang and Eltahir, 2019;

67 Thiery et al., 2017; Bonfils and Lobell, 2007; Sacks et al., 2009). However, many
68 crop models still use air temperature rather than canopy temperature to estimate heat
69 stress; this may overestimate heat stress effects in irrigated cropland (Siebert et al.,
70 2017), since canopy temperature can deviate significantly from air temperature
71 depending on the crop moisture conditions (Siebert et al., 2014). Recently, a
72 comparison of crop model simulated canopy temperatures suggests that most crop
73 models lack a sufficient ability to reproduce the field-measured canopy temperature,
74 even for models with a good performance in grain yield simulation (Webber et al.,
75 2017).

76

77 Satellite-derived land surface temperature (LST) measurements have been used to
78 directly quantify regional scale surface warming or cooling effects resulting from
79 surface energy budget changes due to changes in land cover and land management
80 (Loarie et al., 2011; Tomlinson et al., 2012; Peng et al., 2014). Importantly, yield
81 prediction model comparisons suggest that replacing air temperature with MODIS
82 LST can improve yield predictions because LST accounts for both evaporative
83 cooling and water stress (Li et al., 2019). Satellite data also provide the observational
84 evidence to constrain model performance or directly retrieve crop growth status
85 information. For example, satellite derived soil moisture had been used to characterize
86 irrigation patterns and improve irrigation quantity estimations (Felfelani et al., 2018;
87 Lawston et al., 2017; Jalilvand et al., 2019; Zaussinger et al., 2019). Integration of
88 satellite products like LST therefore have the potential to improve our understanding
89 of how irrigation and climate change impact crop yields, and thus provide guidance
90 for farmers to optimize management decisions.

91

92 In this study, we focused on Nebraska, the third largest maize producer in the United
93 States. Multi-year mean climate data showed that conditions have been drier in
94 western areas and warmer in southern areas of the state (Figure 1a and b).
95 Importantly, Nebraska has historically produced a mixture of irrigated and rainfed
96 maize that facilitated comparison (more than half (56%) of the Nebraska maize
97 cropland was irrigated, with more irrigated maize in the western area (Figure 1c),
98 according to the United States Department of Agriculture (USDA, 2018a)). County
99 yield data from the USDA showed that interannual fluctuations in rainfed maize yield
100 have in general been much larger than for irrigated maize (Figure 1b). Although

101 irrigated yields were higher, rainfed maize yields have grown faster than irrigated (an
102 average of 3.9% per year versus 1.0% per year) over the study period (2003-2016)
103 (Figure 1b), in part because breeding technology progress has improved the drought
104 tolerance of maize hybrids (Messina et al., 2010).

105

106 As noted above, irrigation potentially benefits crop yields by moderating both water
107 and high temperature stress. Here we used satellite-derived LST and satellite-derived
108 water stress metrics to statistically tease apart the contributions of irrigation to water
109 and heat stress alleviation, separately. We: (1) evaluated the difference in temperature
110 and moisture conditions over irrigated and rainfed maize croplands; (2) explored how
111 irrigation mitigated water and high temperature stresses using panel statistical models;
112 (3) quantified the relative contributions of irrigation-induced water and high
113 temperature stress alleviation to yield improvements; and (4) explored whether
114 current crop models reproduced the observed irrigation benefits on maize growth
115 status.

116 **2. Materials and Methods**

117 We first describe the data used, followed by a brief description of statistical
118 methodology.

119 **2.1 Satellite products to identify irrigated and non-irrigated maize areas**

120 We used the United States Department of Agriculture's Cropland Data Layer (CDL)
121 to identify maize croplands for each year in the study period 2003-2016 (USDA,
122 2018b). The irrigation distribution map across Nebraska was obtained from a previous
123 study that used Landsat-derived plant greenness and moisture information to create a
124 continuous annual irrigation map across U.S. Northern High Plains (Deines et al.,
125 2017). The irrigation map showed a very high accuracy (92 to 100%) when validated
126 with randomly generated test points and also highly correlated with county statistics
127 ($R^2 = 0.88-0.96$) (Deines et al., 2017). Both the CDL and irrigation map are at 30m
128 resolution. We first projected them to MODIS sinusoidal projection and then
129 aggregated them to 1km resolution to align with MODIS ET and LST products. Then,
130 pixels containing more than 60% maize and an irrigation fraction >60% were labeled
131 as irrigated maize while pixels with >60% maize and <10% irrigation fraction were
132 labeled as rainfed maize croplands. As always, threshold selection involves a tradeoff

133 between mixing samples and retaining as many samples as possible. Our choices of
134 <10% as the threshold for rainfed maize and 60% to define irrigated maize
135 represented the best optimization in our sample, as we found that more stringent
136 threshold had a very small effect on LST differences between irrigated and rainfed
137 maize at county level but resulted in significant data omission (more details in
138 supplementary Figure 1-2).

139 **2.2 Maize phenology information**

140 Maize growth stage information derived in a previous study was used to assess the
141 influence of irrigation on maize growth during different growth stages (Zhu et al.,
142 2018). Stage information including emergence date, silking date, and maturity date,
143 was derived with MODIS WDRVI (Wide Dynamic Range Vegetation Index, 8-day
144 and 250m resolution) based on a hybrid method combining shape model fitting (SMF)
145 and threshold-based analysis. Then we defined vegetative period (VP) as period from
146 emergence date to silking date, grain filling period (GFP) as period from silking date
147 to maturity date and growing season (GS) as period from emergence date to maturity
148 date. Details can be found in our previous studies (Zhu et al., 2018). WDRVI was
149 used due to its higher sensitivity to changes at high biomass than other vegetation
150 indices (Gitelson et al., 2004) and was estimated with the following equation:

$$151 \quad NDVI = (\rho_{NIR} - \rho_{red}) / (\rho_{NIR} + \rho_{red}) \quad (1)$$

$$152 \quad WDRVI = 100 * \frac{[(\alpha - 1) + (\alpha + 1) \times NDVI]}{[(\alpha + 1) + (\alpha - 1) \times NDVI]} \quad (2)$$

153 where ρ_{red} and ρ_{NIR} were the MODIS surface reflectance in the red and NIR bands,
154 respectively. To minimize the effects of aerosols, we used the 8-day composite
155 products in MOD09Q1 and MYD09Q1 and quality-filtered the reflectance data using
156 the band quality control flags. Only data passing the highest quality control were
157 retained (Zhu et al., 2018). The scaling factor, $\alpha=0.1$, was adopted based on a
158 previous study to degrade the fraction of the NIR reflectance at moderate-to-high
159 green vegetation and best linearly capture the maize green leaf area index (LAI)
160 (Guindin-Garcia et al., 2012).

161 **2.3 Temperature exposure during maize growth**

162 We used daily 1-km spatial resolution MODIS Aqua LST (MYD11A1) data to
163 characterize the crop surface temperature; since its overpassing times are at 1:30 and
164 13:30, it is closer to the times of daily minimum and maximum temperature than the

165 MODIS Terra LST (Wan et al., 2008) and is therefore better for characterizing crop
 166 surface temperature stress (Johnson 2016; Li et al., 2019). For quality control, pixels
 167 with an LST error >3 degree were filtered out based on the corresponding MODIS
 168 LST quality assurance layers. Missing values (less than 3% of total observations)
 169 were interpolated with robust spline function (Teuling et al., 2010). Aqua LST data
 170 are available after July 2002; we thus restricted our study to the period 2003-2016.
 171 For comparison, we also obtained daily minimum and maximum surface air
 172 temperature (Tmin and Tmax) at 1-km resolution from Daymet version 3 (Thornton et
 173 al., 2018). For both MODIS LST and air temperature, we calculated integrated crop
 174 heat exposure -- the growing degree days (GDD) and extreme degree days (EDD) --
 175 according to the following definitions:

176

$$177 \quad GDD_8^{30} = \sum_{t=1}^N DD_t, \quad DD_t = \begin{cases} 0, & \text{when } T < 8^{\circ}\text{C} \\ T - 8, & \text{when } 8^{\circ}\text{C} \leq T < 30^{\circ}\text{C} \\ 22, & \text{when } T \geq 30^{\circ}\text{C} \end{cases} \quad (3)$$

$$178 \quad EDD_{30}^{\infty} = \sum_{t=1}^N DD_t, \quad DD_t = \begin{cases} 0, & \text{when } T < 30^{\circ}\text{C} \\ T - 30, & \text{when } T \geq 30^{\circ}\text{C} \end{cases} \quad (4)$$

179 Here temperature (T) could be either air temperature or LST, interpolated from daily
 180 to hourly values with sine function (Tack et al., 2017). t represents the hourly time
 181 step, N is the total number of hours in a specified growing period (either the entire
 182 growing season, or a specific phenological growth phase, as defined below).
 183 Following previous studies (Lobell et al., 2011; Zhu et al., 2019), we used 30 °C as the
 184 high temperature threshold, although higher values might be applicable in some
 185 settings (Sanchez et al., 2014).

186

187 **2.4 Maize Water Stress**

188 Water stress during maize growth was characterized by the ratio of evapotranspiration
 189 (ET) to potential evapotranspiration (PET), as in a previous study (Mu et al., 2013).
 190 We used MODIS products (MYD16A2) for both ET and PET, based on its good
 191 performance for natural vegetation (Mu et al., 2011); however, our comparison using
 192 flux tower observed ET at an irrigated maize site at Nebraska suggested that ET at the
 193 irrigated maize was significantly underestimated by MODIS ET (Supplementary
 194 Figure 3). We therefore also used another ET product (SSEBop ET) to replace

195 MODIS ET. SSEBop ET was also estimated with MODIS products (Senay et al.,
196 2013), like LST, vegetation index, and albedo as input variables, but used a revised
197 algorithm including predefined boundary conditions for hot and cold reference pixels
198 (Senay et al., 2013) and showed better performance than MODIS ET (Velpuri et al.,
199 2013). We also saw improved performance when we compared it with flux tower
200 observed ET at an irrigated maize site (Supplementary Figure 4). The comparison of
201 MODIS PET and flux tower estimated PET showed satisfactory performance for
202 MODIS PET (Supplementary Figure 5). Since MODIS PET from MYD16A2 has a
203 spatial resolution of 500 m with 8-day temporal resolution, while SSEBop ET has
204 1km spatial resolution with daily time step, we reconciled the two datasets to 1km
205 spatial resolution and 8-day temporal resolution.

206 **2.5 Crop model simulation results**

207 We compared the results of our statistical analysis with four gridded crop models.
208 Simulation results from pAPSIM, pDSSAT, LPJ-GUESS, CLM-crop for both rainfed
209 and irrigated maize across Nebraska were obtained from Agricultural Model
210 Intercomparison and Improvement Project (AgMIP) (Rosenzweig et al., 2013) and
211 Inter-Sectoral Impact Model Intercomparison Project 1 (ISIMIP1) (Warszawski et al.,
212 2014). The four models were driven by the same climate forcing dataset (AgMERRA)
213 and run at a spatial resolution of 0.5 arc-degree longitude and latitude. All simulations
214 were conducted for purely rainfed and near-perfectly irrigated conditions. These
215 models simulated maize yield, total biomass, ET and growing stage information
216 (planting date, flowering date and maturity date). Planting date occurs on the first day
217 following the prescribed sowing date in which soil temperature is at least 2 degrees
218 above the 8 °C base temperature. Harvest occurs once the specified heat units are
219 reached. Heat units to maturity were calibrated from the prescribed crop calendar data
220 (Elliott et al., 2015). Crop model simulation was evaluated by calculating the Pearson
221 correlation between simulated yields in the baseline simulations and detrended
222 historical yields for each country from the Food and Agriculture Organization.
223 Management scenario ‘harmonon’ was selected, meaning the simulation using
224 harmonized fertilizer inputs and assumptions on growing seasons. More details on the
225 simulation protocol can be found in Elliott et al. (2015) and Müller et al. (2019). We
226 used this model comparison project outputs to shed light on how well crop models
227 had simulated the irrigation benefits we identified in different phases of crop growth.

228 **2.6 Method**

229 We used standard panel statistical analysis techniques to identify the impacts of
230 irrigation on maize productivity via heat stress reduction and water stress reduction
231 pathways.

232

233 Comparison of LST, ET, PET, ET/PET, GDD and EDD between irrigated and rainfed
234 maize areas was performed within each county to minimize the effects of other
235 spatially-varying factors, like background temperature and management practices, on
236 surface temperature and evapotranspiration. These biophysical variables (LST, ET,
237 PET, ET/PET, GDD and EDD) averaged over each county were then integrated over
238 vegetative period (VP, from emergence date to silking date), grain filling period (GFP,
239 from silking date to maturity date) and whole growing season (GS, from emergence
240 date to maturity date) so we could evaluate whether and how irrigation had
241 differentially influenced maize growth during early VP and late GFP.

242

243 We further examined how irrigation had changed the sensitivity of maize yield and its
244 components to temperature variation. As done in our previous study (Zhu et al., 2019),
245 we decomposed the total yield variation into three components: biomass growth rate
246 (BGR), growing season length (GSL) and harvest index (HI) based on the following
247 equation:

$$248 \text{Yield} = HI \cdot AGB = HI \cdot BGR \cdot GSL \quad (5)$$

249 Aboveground biomass (AGB) was retrieved through a regression model:

$$250 \text{AGB} = 16.4 \cdot \text{IWDRVI}^{0.8} \quad (6)$$

251 which was built in the previous study through regressing field measured maize AGB
252 against MODIS derived integrated WDRVI (IWDRVI) (Zhu et al., 2019). Then HI
253 could be estimated as Yield/AGB and BGR could be estimated as AGB/GSL. This
254 decomposition allowed us to examine how different crop growth physiological
255 processes responded to external forcing: HI characterizes dry matter partitioning
256 between source organ and sink organ and is mainly related with processes
257 determining grain size and grain weight; BGR is related with physiological processes
258 of daily carbon assimilation rate through photosynthesis and GSL is related with crop
259 phenological development. The uncertainties in AGB estimation results from the
260 parameters in the regression model (Eq. (6)) converting IWDRVI to AGB. Here we
261 quantified the uncertainties rooted in the estimated parameters through running the

262 panel model 1000 times with the samples generated from each parameter's 95%
 263 confidence interval (Zhu et al., 2019).

264

265 Temperature sensitivity of irrigated or rainfed yield (S_T^{Yield}) was estimated using a
 266 panel data model (Eq. (7)) with growing season mean LST and ET/PET as the
 267 explanatory variables:

$$268 \log(Yield_{i,t}) = \gamma_1 t + \gamma_2 LST_{i,t} + \gamma_3 \frac{ET}{PET}_{i,t} + County_i + \varepsilon_{i,t} \quad (7)$$

269 $Yield_{i,t}$ is maize yield (t/ha) in county i and year t . It is a function of overall yield
 270 trends ($\gamma_1 t$) that have fairly steadily increased over the study period (Figure 1b), local
 271 crop temperature stress ($LST_{i,t}$), and local crop water stress ($\frac{ET}{PET}_{i,t}$). The $County_i$
 272 terms provide an independent intercept for each county (fixed effect), and thus
 273 account for time-invariant county-level differences that contributed to variations in

$\frac{\partial \ln(Yield)}{\partial LST}$

274 yield, like the soil quality. $\varepsilon_{i,t}$ is an idiosyncratic error term. γ_2 or $\frac{\partial \ln(Yield)}{\partial LST}$ defines
 275 the temperature sensitivity of yield. The temperature sensitivity of BGR (S_T^{BGR}), HI
 276 (S_T^{HI}) and GSL (S_T^{GSL}) could be estimated with Eq (7) in a similar way through using
 277 BGR, HI and GSL as the dependent variable. Here the dependent variable Yield
 278 (BGR, GSL and HI) was logged, so the estimated temperature sensitivity represented
 279 the percentage change of Yield (BGR, GSL and HI) with 1 °C temperature increase.

280

281 To quantify the relative contribution of water and high temperature stress alleviation
 282 to yield benefit, we related the yield difference between irrigated and non-irrigated
 283 maize (irrigation yield-rainfed yield, $\Delta Yield$) to a quadratic function of growing
 284 season EDD and ET/PET differences between irrigated and rainfed maize:

$$285 \Delta Yield_{i,t} = \gamma_1 \Delta \frac{ET}{PET}_{i,t} + \gamma_2 \Delta \frac{ET}{PET}_{i,t}^2 + \gamma_3 \Delta EDD_{i,t} + \gamma_4 \Delta EDD_{i,t}^2 + County_i + \varepsilon_{i,t} \quad (8)$$

286 The yield improvement explained by heat and water stress alleviation was estimated

$$287 \text{ as } \frac{\gamma_1 \sum \Delta \frac{ET}{PET}_{i,t} + \gamma_2 \sum \Delta \frac{ET}{PET}_{i,t}^2 + \gamma_3 \sum \Delta EDD_{i,t} + \gamma_4 \sum \Delta EDD_{i,t}^2}{\sum \Delta Yield_{i,t}} \quad . \quad \text{The relative}$$

288 contribution of water and high temperature stress alleviation was estimated as

$$\frac{\gamma_1 \sum \Delta \frac{ET}{PET_{i,t}} + \gamma_2 \sum \Delta \frac{ET^2}{PET_{i,t}}}{\gamma_1 \sum \Delta \frac{ET}{PET_{i,t}} + \gamma_2 \sum \Delta \frac{ET^2}{PET_{i,t}} + \gamma_3 \sum \Delta EDD_{i,t} + \gamma_4 \sum \Delta EDD_{i,t}^2}$$

289 and

$$\frac{\gamma_3 \sum \Delta EDD_{i,t} + \gamma_4 \sum \Delta EDD_{i,t}^2}{\gamma_1 \sum \Delta \frac{ET}{PET_{i,t}} + \gamma_2 \sum \Delta \frac{ET^2}{PET_{i,t}} + \gamma_3 \sum \Delta EDD_{i,t} + \gamma_4 \sum \Delta EDD_{i,t}^2},$$

290 respectively. We also

291 ran the model above using daytime LST difference (ΔLST) in lieu of ΔEDD as a
 292 robustness check:

$$\Delta Yield_{i,t} = \gamma_1 \Delta \frac{ET}{PET_{i,t}} + \gamma_2 \Delta \frac{ET^2}{PET_{i,t}} + \gamma_3 \Delta LST_{i,t} + \gamma_4 \Delta LST_{i,t}^2 + County_i + \varepsilon_{i,t} \quad (9)$$

293

294 To diagnose any potential collinearity between $\Delta \frac{ET}{PET}$ and ΔLST , we calculated the
 295 Variance Inflation Factor (VIF) for the model above. In this formulation the relative
 296 contributions of water and high temperature stress alleviation were estimated as

$$\frac{\gamma_1 \sum \Delta \frac{ET}{PET_{i,t}} + \gamma_2 \sum \Delta \frac{ET^2}{PET_{i,t}}}{\gamma_1 \sum \Delta \frac{ET}{PET_{i,t}} + \gamma_2 \sum \Delta \frac{ET^2}{PET_{i,t}} + \gamma_3 \sum \Delta LST_{i,t} + \gamma_4 \sum \Delta LST_{i,t}^2}$$

297 and

$$\frac{\gamma_3 \sum \Delta LST_{i,t} + \gamma_4 \sum \Delta LST_{i,t}^2}{\gamma_1 \sum \Delta \frac{ET}{PET_{i,t}} + \gamma_2 \sum \Delta \frac{ET^2}{PET_{i,t}} + \gamma_3 \sum \Delta LST_{i,t} + \gamma_4 \sum \Delta LST_{i,t}^2},$$

298 respectively.

299 3. Results

300 As expected, irrigation improved maize yield and the yield benefit showed a distinct
 301 spatial variation when we compared areas we identified as irrigated versus rainfed
 302 maize. The yield benefit of irrigation was much higher in the western area of the state
 303 (Figure 2a), because the drier environment in western area featured a wider yield gap
 304 between irrigated and rainfed cropland in an average year. The satellite derived
 305 vegetation index WDRVI reflected these differences, with higher values in areas we
 306 identified as irrigated maize, especially around maize silking (Figure 2b). Importantly,
 307 this suggested that irrigated and rainfed cropland were distinguishable based on
 308 satellite derived crop seasonality information.

309

310 When county-level LST data were averaged over 2003-2016, the daytime LST in
311 irrigated maize was 1.5°C cooler than rainfed maize, while nighttime LST showed a
312 very slight difference (0.2°C) (Figure 3a,b). When the LST differences were
313 integrated over different growing periods (Figure 3e-h), we found that the daytime
314 cooling effect was greatest in the GFP (Figure 3g), probably due to the higher LAI (or
315 ground cover) and transpiration during that stage of growth. This was also consistent
316 with previous field studies showing that irrigation was mainly applied during the
317 middle to late reproductive period, which corresponded to the greatest water demand
318 period (Chen et al., 2018). The spatial pattern of the LST difference showed stronger
319 cooling effect in the western area (Figure 3c-h), which was similar to the spatial
320 pattern of yield benefit identified in Figure 2a. In contrast, surface air temperature
321 showed much smaller daytime cooling effect (Figure 3i,j). The mean daytime and
322 nighttime air temperature differences between irrigated and rainfed maize were -0.2°C
323 and -0.3°C, respectively, and the spatial pattern of air temperature difference over VP
324 and GFP was also relatively small between counties and crop growth periods (Figure
325 3k-p). The difference between spatial-temporal patterns identified using LST and air
326 temperature likely arises because LST reflects canopy energy partition between latent
327 heat flux and sensible heat flux. Additional moisture provided by irrigation results in
328 more heat transferred as latent heat flux, creating a cooling effect.

329

330 Temperature is an important driver of crop phenology and has been used as the
331 primary environmental variable in crop phenology models (Wang et al., 1998). Given
332 the identified irrigation cooling, we further examined how irrigation altered maize
333 phenological stages. We found irrigated maize showed an earlier emergence and
334 silking but delayed maturity (Figure 4a). Consequently, GFP was extended by 7.5
335 days on average, which contributed to most of the total GS extension (8.1 days)
336 (Figure 4b). Site measurements of phenological stage information confirmed that
337 irrigated maize had a longer GS, especially during GFP (Figure 4c). That this
338 extension mainly occurred during GFP could be due to: (1) LST cooling was more
339 prominent during GFP, (2) phenological development during GFP was more sensitive
340 to temperature variation than development during VP (Egli et al., 2004) and (3)
341 variety differences between irrigated and rainfed maize. The spatial pattern suggested
342 GS and GFP extension were more significant in the western area of the state (Figure
343 4g-h), likely due to the corresponding stronger cooling effect.

344

345 We integrated LST or air temperature as described above (Materials and Methods) to
346 estimate total heat exposure (GDD and EDD) over the maize growing season. We
347 found both LST and air temperature estimated GDD were greater in irrigated maize
348 than GDD in rainfed maize across most counties, especially during GFP (Figure 5a,c),
349 which was very likely due to the GFP extension. As GDD characterizes the beneficial
350 thermal time accumulation, the greater GDD in irrigated maize might contribute to the
351 higher yield. In terms of EDD, LST estimated EDD suggested that irrigation
352 suppressed high temperature stress especially for GFP (Figure 5b), while air
353 temperature estimated EDD failed to characterize the irrigation induced lower high
354 temperature stress (Figure 5d).

355

356 SSEBop ET and MODIS PET were used to explore how irrigation influenced water
357 demand and water supply across maize. We found irrigation led to 27% higher
358 ($p < 0.001$) ET and 2% lower ($p > 0.05$) PET (Figure 6a-b). Higher ET was anticipated
359 in irrigated maize, and lower PET might be due to irrigation cooling effect, which
360 resulted in lower VPD and thus lower evaporative demand. We used the ratio of ET to
361 PET as a proxy for water stress in this study, where low values indicated that plants
362 were not transpiring at their full potential in the ambient conditions. This ratio was
363 higher for irrigated maize, especially during the GFP (Figure 6c), and the spatial
364 distribution suggested that the difference was greater in western counties than eastern
365 counties (Figure 6d-e), similar to the distribution of the local cooling effect identified
366 in Figure 3c.

367

368 We divided the temperature sensitivity of yield into three components (sensitivity of
369 BGR, GSL and HI) to investigate how irrigation changed the response of maize
370 physiological processes to temperature. Because collinearity between LST and
371 ET/PET was potentially worrisome, we quantified the variance inflation factor (VIF)
372 in the model; this was found to be well below standard thresholds, with a value of 2.8
373 and 3.6 for irrigated and rainfed maize yield, respectively. (VIFs over 10 indicate
374 strongly collinear variables, with 5 being a more strict standard). As shown in Figure
375 7, we found that temperature sensitivity of yield was significantly weakened from -
376 6.9%/°C ($p < 0.01$) to -1%/°C ($p < 0.01$) in rainfed vs. irrigated areas, and this yield
377 sensitivity change was mainly driven by a change in the sensitivity of the HI, which

378 was weakened from $-4.2\%/^{\circ}\text{C}$ ($p<0.01$) to $1\%/^{\circ}\text{C}$ ($p<0.01$). In both rainfed and
379 irrigated maize, temperature sensitivity of GSL was quite close (approximately -
380 $2\%/^{\circ}\text{C}$ ($p<0.01$)), while BGR was only slightly influenced by temperature (Figure 7).

381

382 We found that irrigation not only lowered water and high temperature stress, but also
383 made yield less sensitive to water and high temperature stress (Figure 8a-c),
384 consistent with previous studies (Troy et al., 2015; Tack et al., 2017). For example,
385 field data across Africa suggests that better water management can reduce yield loss
386 due to heat stress from -1.7% per degree days to -1% per degree days (Lobell et al.,
387 2011). We statistically related yield differences to climatic variables differences using
388 the linear model (Eq. (8)), and estimated that $61 \pm 9.4\%$ of yield improvement between
389 irrigated and rainfed maize could be explained by the irrigation induced heat and
390 water stress alleviation. We further calculated that $79 \pm 13\%$ of that yield improvement
391 was due to water stress alleviation and $21 \pm 3.2\%$ was due to heat stress alleviation.
392 Because the distribution of ΔEDD was truncated for points with $\Delta\text{EDD}>0$ (Figure 8e),
393 we explored an alternative model with quadratic functions of ΔLST and $\Delta\text{ET}/\text{PET}$
394 (Eq. (9)). In this specification, $72 \pm 12\%$ of yield improvement was explained by water
395 and high temperature stress alleviation, with $65 \pm 10\%$ and $35 \pm 5.3\%$ of yield
396 improvement due to water and high temperature stress alleviation, respectively. We
397 also estimated VIF in the model; this was found to be well below standard thresholds,
398 with a value of 2.2. Intuitively, our low VIF value was likely due to the use of
399 differences in LST and ET/PET between irrigated and rainfed maize, rather than
400 directly using LST and ET/PET as the explanatory variables. We also note that the
401 high temperature stress alleviation estimated here appears larger than the estimation in
402 a recent study (Li et al., 2020) where LST was also employed to detect the yield
403 benefit of irrigation cooling effect. But this is due to the fact that we estimated cooling
404 effect benefits relative to total sum of cooling and water stress effects, whereas Li et
405 al. calculated cooling effect relative to net yield differences between irrigated and
406 rainfed maize. Since other effects (like cultivar difference and fertilizer application)
407 might also contribute to the yield difference between irrigated and rainfed maize, the
408 denominator used in Li et al., (2020) was larger.

409

410 Because we found a strong effect on yields via alleviation of heat stress (and not
411 simply water stress), we compared our results with four process-based crop models

412 that simulated crop growth under both rainfed and irrigated conditions. These
413 simulations qualitatively reproduced the irrigation-induced higher maize yield,
414 biomass, and ET (Figure 9), but to different degrees. The highest modeled
415 improvement was identified in CLM-crop, with increases of 57%, 43% and 32% in
416 yield, biomass and ET, respectively. However, all models except CLM-crop failed to
417 reproduce the growing stage extension under irrigation (Figure 9), likely because
418 CLM-crop was the only one of the tested models to have implemented a canopy
419 energy balance module to simulate canopy temperature. CLM-crop was thus the only
420 model able to capture the irrigation-induced evaporative cooling effect (heat-stress
421 reduction). That the best agreement between observed and modeled results occurred
422 with the only model that plausibly accounted for heat-stress alleviation due to
423 irrigation was further evidence that this was the phenomenon we captured in our
424 satellite observational study.

425 **4. Discussion and conclusion**

426 By integrating satellite products and ground-based information on cropping and
427 irrigation, we showed that irrigated maize yields were higher than rainfed maize
428 yields because added irrigation water reduced heat stress in addition to water stress.
429 Our study underlines the relative importance of heat stress alleviation in yield
430 improvement and the necessity of incorporating crop canopy temperature models to
431 better characterize heat stress impacts on crop yields (Teixeira et al., 2013; Kar and
432 Kumar, 2007). In addition, disentangling the two effects allows crop models to better
433 predict crop phenology, considering irrigation induced cooling effect alters maize
434 growing phases.

435

436 Although ours is not the first study to suggest replacing air temperature with MODIS
437 LST for maize yield prediction, especially under extreme warm and dry conditions,
438 our results underscore important implications of doing so. Given the important role of
439 heat stress in determining crop yield, thermal band derived LST information at finer
440 spatial and temporal resolution should be a critical input for satellite data driven yield
441 prediction models (Wang et al., 2015; Huryňa et al., 2019; Li et al., 2019; Meerdink et
442 al., 2019). In addition, given the differential responses of crop growth to heat and

443 water stresses in different stages, fusing satellite derived crop stage information with
444 the heat and water stressors might improve crop yield prediction.

445

446 This study also has useful implications for process-based crop model development. In
447 our model evaluation, only the model that had implemented a canopy energy balance
448 scheme captured the observed maize growth stage extension. Our results suggest that
449 the heat stress alleviation due to irrigation identified here is largely overlooked in
450 current crop models. As such, when those crop models are calibrated to match
451 observed yields, processes associated with water stress alleviation are probably
452 overestimated, resulting in uncertainties for predicting future irrigation water demand
453 and crop yield. These uncertainties might mislead future adaptation decisions due to
454 incomplete or biased estimates of the relative contributions of heat and water stress.

455

456 Relatedly, recent studies compared heat stress representation in crops models which
457 explicitly simulate canopy temperature (Webber et al., 2017). For example, STICS
458 estimates canopy temperature using canopy energy balances which account for net
459 radiation, soil heat flux, evapotranspiration and aerodynamic resistance (Brisson et al.,
460 2003). In APSIM, canopy temperature is taken as 6 °C higher than air temperature
461 when the crop is fully stressed and 6 °C cooler than air temperature when the crop is
462 fully transpiring. Between these limits, the basis of the expression for canopy
463 temperature is the relationship between temperature difference (canopy temperature
464 minus air temperature) and the ratio of actual and potential evapotranspiration
465 (Webber et al., 2017). This model comparison study suggests that models using
466 canopy temperature to account for heat stress effects indeed outperform those models
467 depending on air temperature but the model comparison also identified a wide range
468 for the simulated canopy temperature in current crop models. Therefore, assimilating
469 satellite derived LST might be a potential solution to improving crop models heat
470 stress representation so that they can better reproduce the observed heat stress effects
471 (Meng et al., 2009; Xu et al., 2011). These remotely sensed LST can also be used to
472 validate model simulated LST, especially given that the recent ECOSystem
473 Spaceborne Thermal Radiometer Experiment on Space Station (ECOSTRESS)
474 mission makes hourly plant temperature measurement available (Meerdink et al.,
475 2019). However, it is worth noting that the availability of satellite LST presents a
476 constraint when thinking about future climate change impact studies. In addition,

477 some caution is required for validating model-simulated LST, since LST is sensor-
478 and satellite- specific.

479

480 Several limitations and caveats apply to our study. First, the daily MODIS daytime
481 LST we used to explain crop maximum daily temperature had missing values due to
482 quality control checks, and was derived from a mix of crop covers and other land
483 surface temperature information, which might bias the identified irrigation cooling
484 effect. Specifically, using MODIS daytime LST as a proxy for true (measured)
485 maximum crop surface temperature in an empirical statistical model might
486 underestimate the benefit of cooling effect (measurement error in a predictor variable
487 producing attenuation bias). These uncertainties in LST dataset might be resolved
488 with the recently launched ECOSTRESS mission, as its hourly revisiting frequency
489 enables better estimation of maximum daily temperature. The second issue is that
490 water stress and heat stress are not perfectly separable. As what we have shown, the
491 cooling effect of irrigation lowers evaporative demand (PET) and thus indirectly
492 contributes to lower water stress (higher ET/PET). In addition, water stress reduced
493 photosynthesis and ET, resulting in higher plant temperature. Our disentangling
494 methods do not account for the water stress and heat stress interaction effects, so these
495 “heat” and “water stress” channels should be interpreted carefully. We note that our
496 statistical model estimated temperature coefficient should be interpreted as the net of
497 all effects raising surface temperature. The third issue is that our study only examined
498 maize in one state, Nebraska. Although Nebraska is the largest irrigated maize
499 producer in the US, results might differ for other crop types and other landscapes, due
500 to different crop canopy structures and management practices (Chen et al., 2018), and
501 spatial variations in water and heat stresses mitigation effects (Figure 3 and Figure 7).

502

503 Overall, our study suggests that heat stress alleviation, in addition to water stress
504 alleviation, plays an important role in improving irrigated maize yield. Since current
505 models generally cannot accurately simulate the canopy temperature, the irrigation
506 induced yield benefit might have been overly attributed to water stress alleviation.
507 This might bias the future yield prediction under irrigation, since high temperature
508 stress might be more dominant than drought for crop yield formation under future
509 warmer climate (Zhu et al, 2019; Jin et al., 2017). Better constrained crop models --
510 perhaps through integration of satellite observed land surface temperature and crop

511 stage information -- will be necessary to improve yield prediction and help
512 policymakers and farmers make better decisions about where and when to implement
513 irrigation.

514

515 **Code/Data availability**

516 All data related to this paper, along with code for interpretation of data are available
517 upon request from the corresponding author.

518 **Author contribution**

519 All co-authors designed the overall study. Peng Zhu performed the analysis and
520 prepared the manuscript. All co-authors contributed to the interpretation of the results
521 and writing of the paper.

522

523 **Competing interests**

524 The authors declare that they have no conflict of interest.

525

526 **References**

- 527 Autovino, D., Minacapilli, M. and Provenzano, G.: Modelling bulk surface resistance
528 by MODIS data and assessment of MOD16A2 evapotranspiration product in an
529 irrigation district of Southern Italy, *Agric. Water Manag.*, 167, 86–94,
530 doi:10.1016/j.agwat.2016.01.006, 2016.
- 531 Bonfils, C. and Lobell, D.: Empirical evidence for a recent slowdown in irrigation-
532 induced cooling, *Proc. Natl. Acad. Sci. U. S. A.*, 104(34), 13582–13587,
533 doi:10.1073/pnas.0700144104, 2007.
- 534 Bruinsma, J.: The resource outlook to 2050: by how much do land, water and crop
535 yields need to increase by 2050?
536 <ftp://ftp.fao.org/docrep/fao/012/ak971e/ak971e00.pdf>, 2009.
- 537 Brisson, N., Gary, C., Justes, E., Roche, R., Mary, B., Ripoche, D., Zimmer, D.,
538 Sierra, J., Bertuzzi, P., Burger, P., Bussi ère, F., Cabidoche, Y. M., Cellier, P.,
539 Debaeke, P., Gaudill ère, J. P., H énault, C., Maraux, F., Seguin, B. and Sinoquet,
540 H.: An overview of the crop model STICS, in *European Journal of Agronomy*,
541 vol. 18, pp. 309–332., 2003.
- 542 Chen, F., Xu, X., Barlage, M., Rasmussen, R., Shen, S., Miao, S. and Zhou, G.:
543 Memory of irrigation effects on hydroclimate and its modeling challenge,
544 *Environ. Res. Lett.*, 13(6), doi:10.1088/1748-9326/aab9df, 2018.
- 545 Deines, J. M., Kendall, A. D. and Hyndman, D. W.: Annual Irrigation Dynamics in
546 the U.S. Northern High Plains Derived from Landsat Satellite Data, *Geophys.*
547 *Res. Lett.*, 44(18), 9350–9360, doi:10.1002/2017GL074071, 2017.
- 548 DeLucia, E. H., Chen, S., Guan, K., Peng, B., Li, Y., Gomez-Casanovas, N., Kantola,
549 I. B., Bernacchi, C. J., Huang, Y., Long, S. P. and Ort, D. R.: Are we
550 approaching a water ceiling to maize yields in the United States?, *Ecosphere*,
551 10(6), doi:10.1002/ecs2.2773, 2019.
- 552 Egli, D. B.: Seed- Fill Duration and Yield Of Grain Crops, *Adv. Agron.*, 83(C), 243–
553 279, doi:10.1016/S0065-2113(04)83005-0, 2004.
- 554 Elliott, J., Müller, C., Deryng, D., Chryssanthacopoulos, J., Boote, K. J., B üchner, M.,
555 Foster, I., Glotter, M., Heinke, J., Iizumi, T., Izaurralde, R. C., Mueller, N. D.,
556 Ray, D. K., Rosenzweig, C., Ruane, A. C. and Sheffield, J.: The Global Gridded
557 Crop Model intercomparison: data and modeling protocols for Phase 1 (v1.0),
558 *Geosci. Model Dev.*, 8, 261–277. <https://doi.org/10.5194/gmd-8-261-2015>

559 Felfelani, F., Pokhrel, Y., Guan, K. and Lawrence, D. M.: Utilizing SMAP Soil
560 Moisture Data to Constrain Irrigation in the Community Land Model, *Geophys.*
561 *Res. Lett.*, 45(23), 12,892-12,902, doi:10.1029/2018GL080870, 2018..

562 Gitelson, A. A.: Wide Dynamic Range Vegetation Index for Remote Quantification of
563 Biophysical Characteristics of Vegetation, *J. Plant Physiol.*, 161(2), 165–173,
564 doi:10.1078/0176-1617-01176, 2004.

565 Howell, T. A.: Enhancing water use efficiency in irrigated agriculture, *Agron J*, vol.
566 93, pp. 281–289., 2001.

567 Huryňa, H., Cohen, Y., Karnieli, A., Panov, N., Kustas, W. P. and Agam, N.:
568 Evaluation of TsHARP utility for thermal sharpening of Sentinel-3 satellite
569 images using Sentinel-2 visual imagery, *Remote Sens.*, 11(19),
570 doi:10.3390/rs11192304, 2019.

571 Jalilvand, E., Tajrishy, M., Ghazi Zadeh Hashemi, S. A. and Brocca, L.:
572 Quantification of irrigation water using remote sensing of soil moisture in a
573 semi-arid region, *Remote Sens. Environ.*, 231, doi:10.1016/j.rse.2019.111226,
574 2019.

575 Jin, Z., Zhuang, Q., Wang, J., Archontoulis, S. V., Zobel, Z. and Kotamarthi, V. R.:
576 The combined and separate impacts of climate extremes on the current and future
577 US rainfed maize and soybean production under elevated CO₂, *Glob. Chang.*
578 *Biol.*, 23(7), 2687–2704, doi:10.1111/gcb.13617, 2017.

579 Johnson, D. M.: A comprehensive assessment of the correlations between field crop
580 yields and commonly used MODIS products, *Int. J. Appl. Earth Obs. Geoinf.*,
581 52, 65–81, doi:10.1016/j.jag.2016.05.010, 2016.

582 Kang, S. and Eltahir, E. A. B.: Impact of Irrigation on Regional Climate Over Eastern
583 China, *Geophys. Res. Lett.*, 46(10), 5499–5505, doi:10.1029/2019GL082396,
584 2019.

585 Kar, G. and Kumar, A.: Surface energy fluxes and crop water stress index in
586 groundnut under irrigated ecosystem, *Agric. For. Meteorol.*, 146(1–2), 94–106,
587 doi:10.1016/j.agrformet.2007.05.008, 2007.

588 Ke, Y., Im, J., Park, S. and Gong, H.: Downscaling of MODIS One kilometer
589 evapotranspiration using Landsat-8 data and machine learning approaches,
590 *Remote Sens.*, 8(3), doi:10.3390/rs8030215, 2016.

591 Lawston, P. M., Santanello, J. A. and Kumar, S. V.: Irrigation Signals Detected From
592 SMAP Soil Moisture Retrievals, *Geophys. Res. Lett.*, 44(23), 11,860-11,867,
593 doi:10.1002/2017GL075733, 2017.

594 Li, Y., Guan, K., Yu, A., Peng, B., Zhao, L., Li, B. and Peng, J.: Toward building a
595 transparent statistical model for improving crop yield prediction: Modeling
596 rainfed corn in the U.S, *F. Crop. Res.*, 234, 55–65,
597 doi:10.1016/j.fcr.2019.02.005, 2019.

598 Loarie, S. R., Lobell, D. B., Asner, G. P., Mu, Q. and Field, C. B.: Direct impacts on
599 local climate of sugar-cane expansion in Brazil, *Nat. Clim. Chang.*, 1(2), 105–
600 109, doi:10.1038/nclimate1067, 2011.

601 Lobell D B, Bänziger M, Magorokosho C, et al. Nonlinear heat effects on African
602 maize as evidenced by historical yield trials[J]. *Nature climate change*, 2011,
603 1(1): 42-45.

604 Meerdink, S. K., Hook, S. J., Roberts, D. A. and Abbott, E. A.: The ECOSTRESS
605 spectral library version 1.0, *Remote Sens. Environ.*, 230,
606 doi:10.1016/j.rse.2019.05.015, 2019.

607 Meng, C. L., Li, Z. L., Zhan, X., Shi, J. C. and Liu, C. Y.: Land surface temperature
608 data assimilation and its impact on evapotranspiration estimates from the
609 common land model, *Water Resour. Res.*, 45(2), doi:10.1029/2008WR006971,
610 2009.

611 Messina, C. D., Podlich, D., Dong, Z., Samples, M. and Cooper, M.: Yield-trait
612 performance landscapes: From theory to application in breeding maize for
613 drought tolerance, *J. Exp. Bot.*, 62(3), 855–868, doi:10.1093/jxb/erq329, 2011.

614 Mu, Q., Zhao, M. and Running, S. W.: Improvements to a MODIS global terrestrial
615 evapotranspiration algorithm, *Remote Sens. Environ.*, 115(8), 1781–1800,
616 doi:10.1016/j.rse.2011.02.019, 2011.

617 Mu, Q., Zhao, M., Kimball, J. S., McDowell, N. G. and Running, S. W.: A remotely
618 sensed global terrestrial drought severity index, *Bull. Am. Meteorol. Soc.*, 94(1),
619 83–98, doi:10.1175/BAMS-D-11-00213.1, 2013.

620 Müller, C., Elliott, J., Kelly, D., Arneith, A., Balkovic, J., Ciais, P., Deryng, D.,
621 Folberth, C., Hoek, S., Izaurralde, R. C., Jones, C. D., Khabarov, N., Lawrence,
622 P., Liu, W., Olin, S., Pugh, T. A. M., Reddy, A., Rosenzweig, C., Ruane, A. C.,
623 Sakurai, G., Schmid, E., Skalsky, R., Wang, X., de Wit, A. and Yang, H.: The

624 Global Gridded Crop Model Intercomparison phase 1 simulation dataset, *Sci.*
625 *Data*, 6(1), doi:10.1038/s41597-019-0023-8, 2019.

626 Niu, J., Shen, C., Li, S. G. and Phanikumar, M. S.: Quantifying storage changes in
627 regional Great Lakes watersheds using a coupled subsurface-land surface process
628 model and GRACE, MODIS products, *Water Resour. Res.*, 50(9), 7359–7377,
629 doi:10.1002/2014WR015589, 2014.

630 Peng, S. S., Piao, S., Zeng, Z., Ciais, P., Zhou, L., Li, L. Z. X., Myneni, R. B., Yin, Y.
631 and Zeng, H.: Afforestation in China cools local land surface temperature, *Proc.*
632 *Natl. Acad. Sci. U. S. A.*, 111(8), 2915–2919, doi:10.1073/pnas.1315126111,
633 2014.

634 Rosegrant, M.W., Cai, X. and Cline, S.: *World Water and Food to 2025: Dealing*
635 *with Scarcity*, *Food Policy*. <https://doi.org/10.1098/rstb.2005.1744>, 2002.

636 Ruiz-Vera, U.M., Siebers, M.H., Jaiswal, D., Ort, D.R. and Bernacchi, C.J.: Canopy
637 warming accelerates development in soybean and maize, offsetting the delay in
638 soybean reproductive development by elevated CO₂ concentrations. *Plant Cell*
639 *Environ.* 41, 2806–2820. <https://doi.org/10.1111/pce.13410>, 2018.

640 Running, S.W., Mu, Q., Zhao, M. and Moreno, A.: Modis Global Terrestrial
641 Evapotranspiration (ET) Product (NASA MOD16A2/A3) NASA Earth
642 Observing System Modis Land Algorithm. NASA: Washington, DC, USA.

643 Russo, S., Dosio, A., Graversen, R. G., Sillmann, J., Carrao, H., Dunbar, M. B.,
644 Singleton, A., Montagna, P., Barbola, P. and Vogt, J. V.: Magnitude of extreme
645 heat waves in present climate and their projection in a warming world, *J.*
646 *Geophys. Res. Atmos.*, 119(22), 12,500–12,512, doi:10.1002/2014JD022098,
647 2014.

648 Sacks, W. J., Cook, B. I., Buening, N., Levis, S. and Helkowski, J. H.: Effects of
649 global irrigation on the near-surface climate, *Clim. Dyn.*, 33(2–3), 159–175,
650 doi:10.1007/s00382-008-0445-z, 2009.

651 Sanchez, B., Rasmussen, A. and Porter, J.R. (2014). Temperatures and the growth and
652 development of maize and rice: a review. *Global Change Biology* 20, 408–417.

653 Senay, G. B., Bohms, S., Singh, R. K., Gowda, P. H., Velpuri, N. M., Alemu, H. and
654 Verdin, J. P.: Operational Evapotranspiration Mapping Using Remote Sensing
655 and Weather Datasets: A New Parameterization for the SSEB Approach, *J. Am.*
656 *Water Resour. Assoc.*, 49(3), 577–591, doi:10.1111/jawr.12057, 2013.

657 Siebert, S. and Döll, P.: Quantifying blue and green virtual water contents in global
658 crop production as well as potential production losses without irrigation, *J.*
659 *Hydrol.*, 384(3–4), 198–217, doi:10.1016/j.jhydrol.2009.07.031, 2010.

660 Siebert, S., Webber, H., Zhao, G. and Ewert, F.: Heat stress is overestimated in
661 climate impact studies for irrigated agriculture, *Environ. Res. Lett.*, 12(5),
662 doi:10.1088/1748-9326/aa702f, 2017.

663 Siebert, S., Ewert, F., Eyshi Rezaei, E., Kage, H. and Graß R.: Impact of heat stress
664 on crop yield - On the importance of considering canopy temperature, *Environ.*
665 *Res. Lett.*, 9(4), doi:10.1088/1748-9326/9/4/044012, 2014.

666 Tack, J., Barkley, A. and Hendricks, N.: Irrigation offsets wheat yield reductions from
667 warming temperatures, *Environ. Res. Lett.*, 12(11), doi:10.1088/1748-
668 9326/aa8d27, 2017.

669 Teixeira, E. I., Fischer, G., Van Velthuisen, H., Walter, C. and Ewert, F.: Global hot-
670 spots of heat stress on agricultural crops due to climate change, *Agric. For.*
671 *Meteorol.*, 170, 206–215, doi:10.1016/j.agrformet.2011.09.002, 2013.

672 Teuling, A. J., Seneviratne, S. I., Stöckli, R., Reichstein, M., Moors, E., Ciais, P.,
673 Luysaert, S., Van Den Hurk, B., Ammann, C., Bernhofer, C., Dellwik, E.,
674 Gianelle, D., Gielen, B., Grünwald, T., Klumpp, K., Montagnani, L., Moureaux,
675 C., Sottocornola, M. and Wohlfahrt, G.: Contrasting response of European forest
676 and grassland energy exchange to heatwaves, *Nat. Geosci.*, 3(10), 722–727,
677 doi:10.1038/ngeo950, 2010.

678 Thiery, W., Davin, E. L., Lawrence, D. M., Hirsch, A. L., Hauser, M. and
679 Seneviratne, S. I.: Present-day irrigation mitigates heat extremes, *J. Geophys.*
680 *Res.*, 122(3), 1403–1422, doi:10.1002/2016JD025740, 2017.

681 Thornton, P. E., Thornton, M. M., Mayer, B. W., Wei, Y., Devarakonda, R., Vose, R.
682 S. and Cook, R. B.: Daymet: Daily Surface Weather Data on a 1-km Grid for
683 North America, Version 3, Version 3. ORNL DAAC, Oak Ridge, Tennessee,
684 USA [online] Available from: <https://search.earthdata.nasa.gov/search>, 2018.

685 Tomlinson, C. J., Chapman, L., Thornes, J. E. and Baker, C. J.: Derivation of
686 Birmingham’s summer surface urban heat island from MODIS satellite images,
687 *Int. J. Climatol.*, 32(2), 214–224, doi:10.1002/joc.2261, 2012.

688 Troy, T. J., Kipgen, C. and Pal, I.: The impact of climate extremes and irrigation on
689 US crop yields, *Environ. Res. Lett.*, 10(5), doi:10.1088/1748-9326/10/5/054013,
690 2015

691 US Department of Agriculture (USDA) NASS: Quick Stats: Agricultural Statistics
692 Data Base, Natl. Agric. Stat. Serv., Available from:
693 <http://www.nass.usda.gov/QuickStats/>, 2018a.

694 US Department of Agriculture (USDA): Crop Scape and Cropland Data Layer –
695 National Download.
696 https://www.nass.usda.gov/Research_and_Science/Cropland/Release/index.php.
697 2018b

698 Velpuri, N. M., Senay, G. B., Singh, R. K., Bohms, S. and Verdin, J. P.: A
699 comprehensive evaluation of two MODIS evapotranspiration products over the
700 conterminous United States: Using point and gridded FLUXNET and water
701 balance ET, *Remote Sens. Environ.*, 139, 35–49, doi:10.1016/j.rse.2013.07.013,
702 2013.

703 Wallace, J. S.: Increasing agricultural water use efficiency to meet future food
704 production, *Agric. Ecosyst. Environ.*, 82(1–3), 105–119, doi:10.1016/S0167-
705 8809(00)00220-6, 2000.

706 Wan, Z.: New refinements and validation of the MODIS Land-Surface
707 Temperature/Emissivity products, *Remote Sens. Environ.*, 112(1), 59–74,
708 doi:10.1016/j.rse.2006.06.026, 2008.

709 Wang, E. and Engel, T.: Simulation of phenological development of wheat crops,
710 *Agric. Syst.*, 58(1), 1–24, doi:10.1016/S0308-521X(98)00028-6, 1998.

711 Wang, F., Qin, Z., Song, C., Tu, L., Karnieli, A. and Zhao, S.: An improved mono-
712 window algorithm for land surface temperature retrieval from landsat 8 thermal
713 infrared sensor data, *Remote Sens.*, 7(4), 4268–4289, doi:10.3390/rs70404268,
714 2015.

715 Webber, H., Martre, P., Asseng, S., Kimball, B., White, J., Ottman, M., Wall, G. W.,
716 De Sanctis, G., Doltra, J., Grant, R., Kassie, B., Maiorano, A., Olesen, J. E.,
717 Ripoche, D., Rezaei, E. E., Semenov, M. A., Stratonovitch, P. and Ewert, F.:
718 Canopy temperature for simulation of heat stress in irrigated wheat in a semi-arid
719 environment: A multi-model comparison, *F. Crop. Res.*, 202, 21–35,
720 doi:10.1016/j.fcr.2015.10.009, 2017.

721 Xu, T., Liu, S., Liang, S. and Qin, J.: Improving predictions of water and heat fluxes
722 by assimilating MODIS land surface temperature products into the Common
723 Land Model, *J. Hydrometeorol.*, 12(2), 227–244, doi:10.1175/2010JHM1300.1,
724 2011.

725 Zaussinger, F., Dorigo, W., Gruber, A., Tarpanelli, A., Filippucci, P. and Brocca, L.:
726 Estimating irrigation water use over the contiguous United States by combining
727 satellite and reanalysis soil moisture data, *Hydrol. Earth Syst. Sci.*, 23(2), 897–
728 923, doi:10.5194/hess-23-897-2019, 2019.

729 Zhu, P., Jin, Z., Zhuang, Q., Ciais, P., Bernacchi, C., Wang, X., Makowski, D. and
730 Lobell, D.: The important but weakening maize yield benefit of grain filling
731 prolongation in the US Midwest, *Glob. Chang. Biol.*, 24(10), 4718–4730,
732 doi:10.1111/gcb.14356, 2018.

733 Zhu, P., Zhuang, Q., Archontoulis, S. V., Bernacchi, C. and Müller, C.: Dissecting the
734 nonlinear response of maize yield to high temperature stress with model-data
735 integration, *Glob. Chang. Biol.*, 25(7), 2470–2484, doi:10.1111/gcb.14632,
736 2019.

737

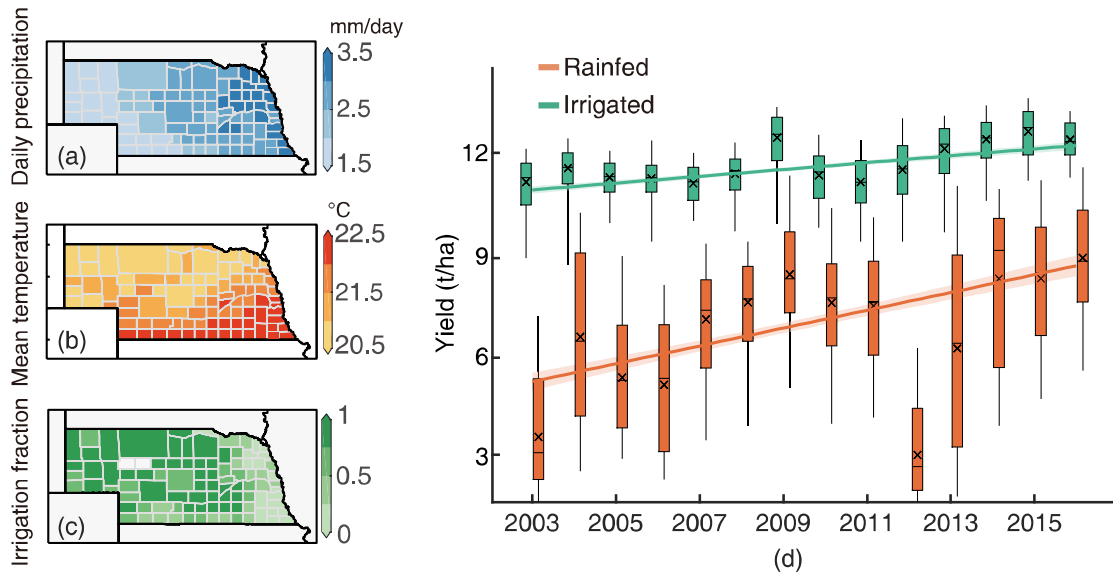
738 **Acknowledgments**

739

740 We thank the NSF/USDA NIFA INFEWS T1 #1639318 for funding support.

741

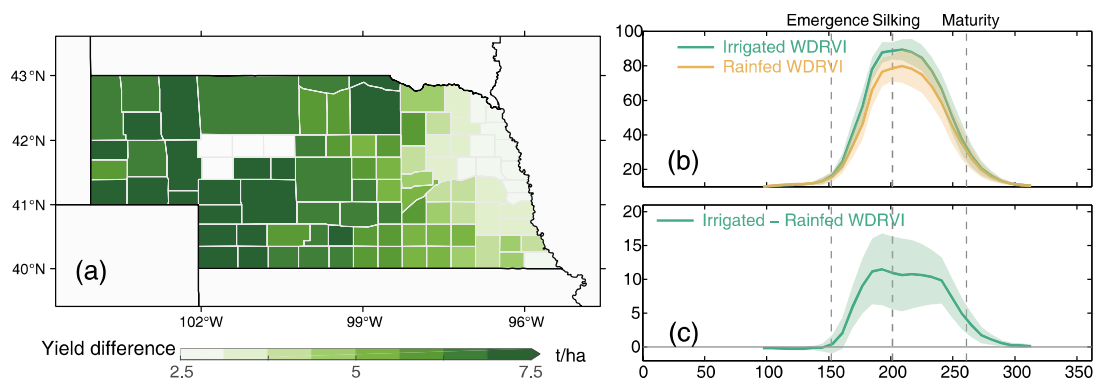
742 **Figures**



743

744 **Figure 1:** The spatial pattern of county level multi-year (2003-2016) mean daily
 745 precipitation (a) and air temperature (b) during maize growing season. County level
 746 multi-year (2003-2016) mean maize irrigation fraction across Nebraska (c). The
 747 maize irrigation fraction is based on USDA NASS report. Boxplot of county level
 748 irrigated and rainfed maize yield in Nebraska over the study period (d). The lines in (d)
 749 show the linear fitted yield trend with 95% confidence interval. Boxplots indicate the
 750 median (horizontal line), mean (cross), inter-quartile range (box), and 5–95th
 751 percentile (whiskers) of rainfed or irrigated yield across all counties.

752

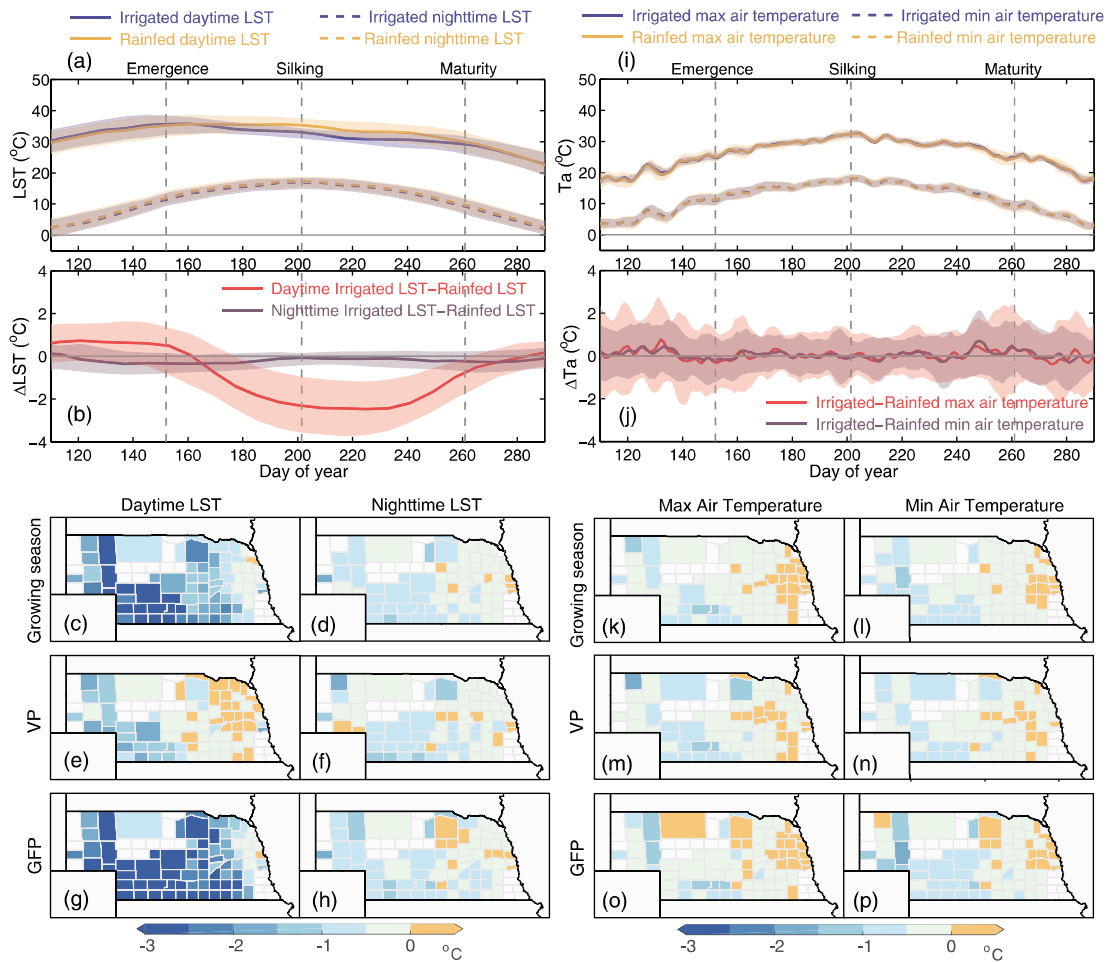


753

754 **Figure 2:** The difference between irrigated and rainfed maize yield (a) and satellite
 755 observed vegetation index (b and c). The shaded area in (b) and (c) shows one
 756 standard deviation of WDRVI (b) and WDRVI difference (c).

757

758

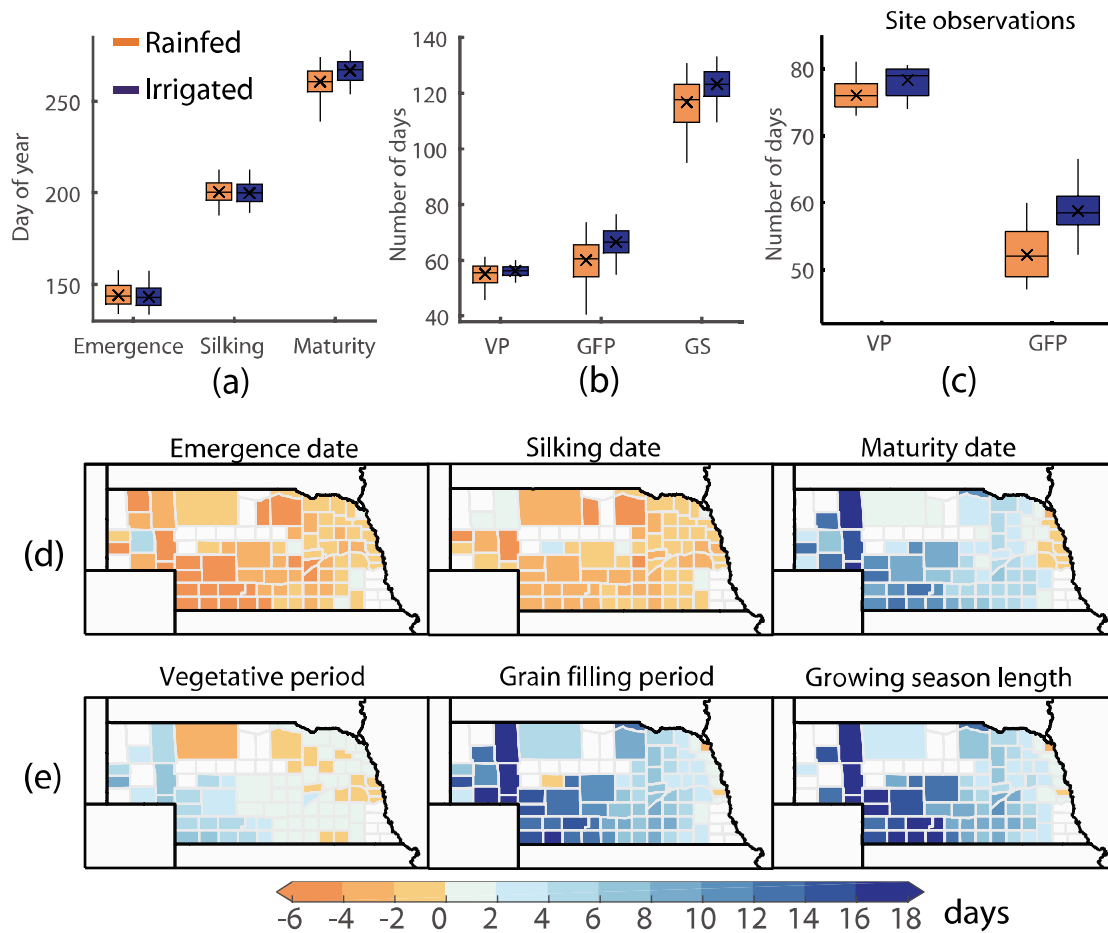


759

760 **Figure 3:** Spatial-temporal patterns of daytime and nighttime MODIS LST
 761 differences (left panel, a-h) and surface air temperature differences (right panel, i-p)
 762 between irrigated and rainfed maize in different growth stages: vegetative period and
 763 grain filling period. The shaded areas in (a), (b) and (i), (j) show one standard
 764 deviation of corresponding variables.

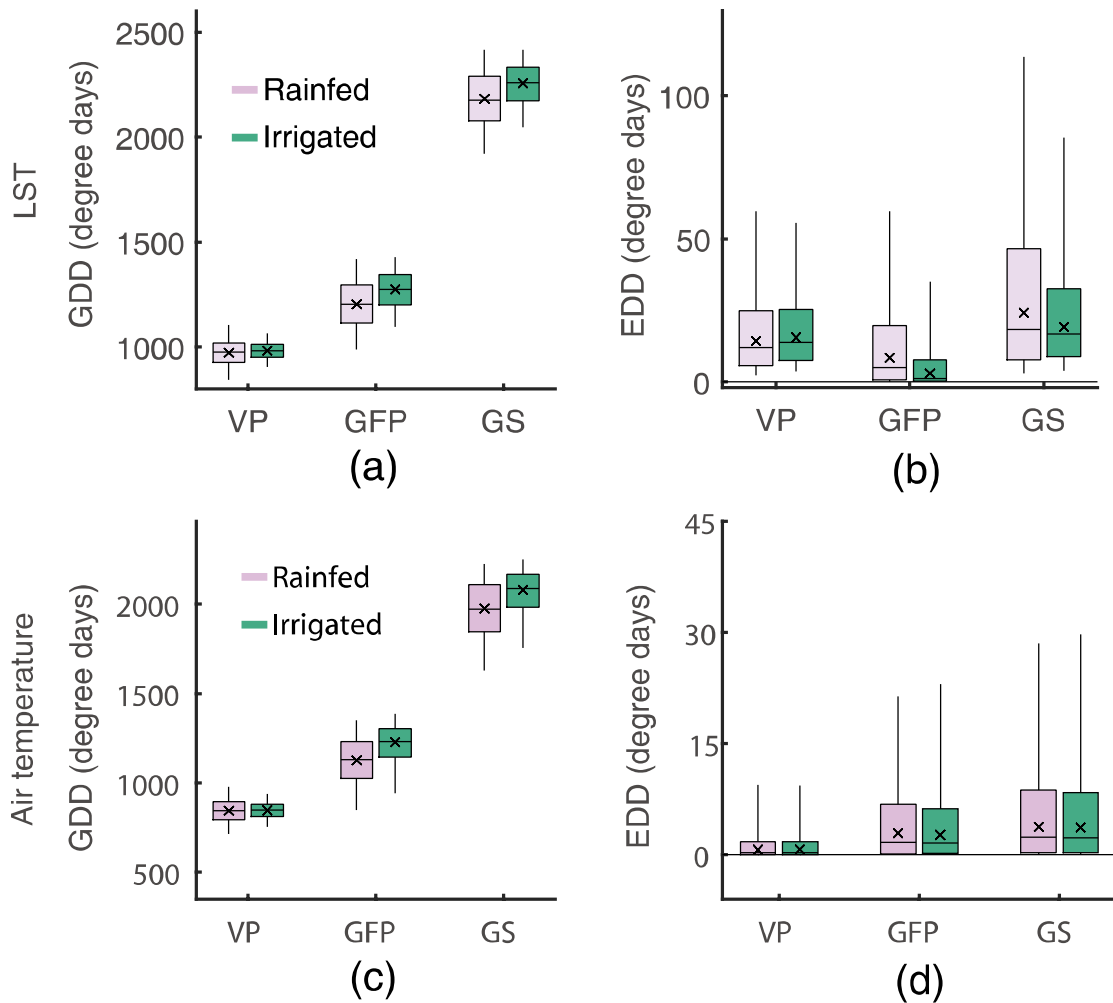
765

766



767
 768
 769
 770
 771
 772

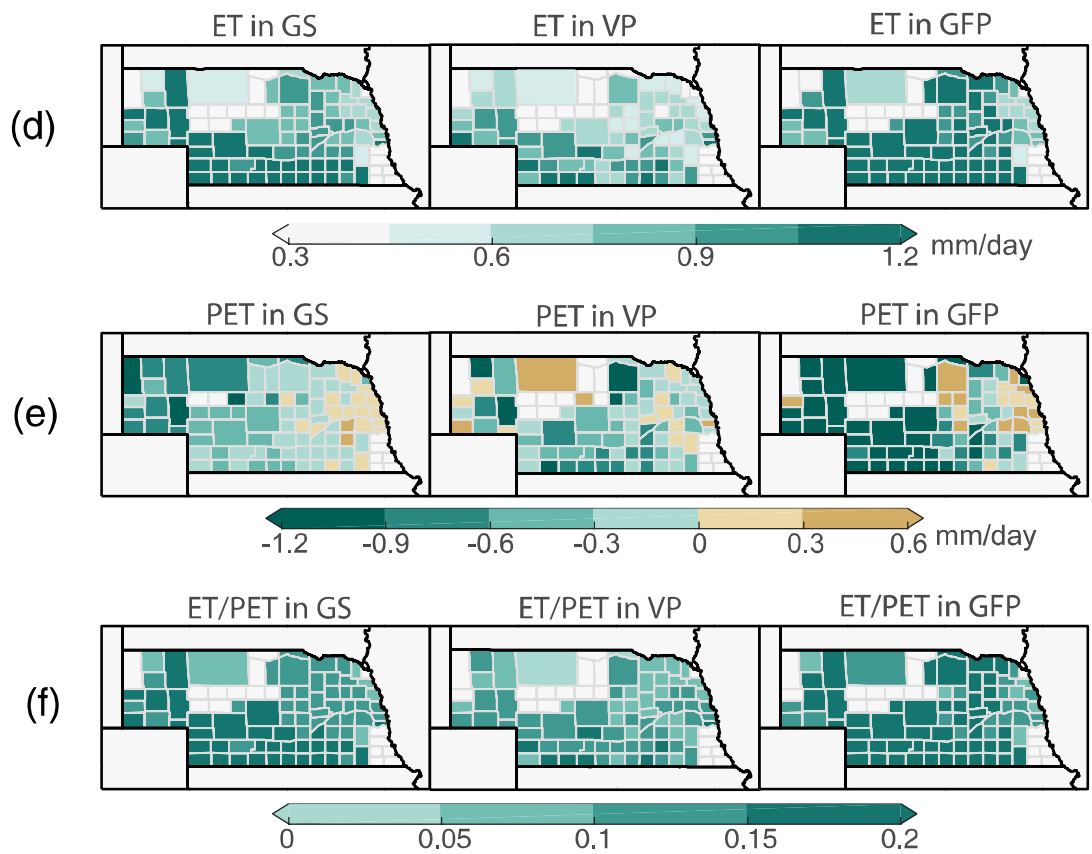
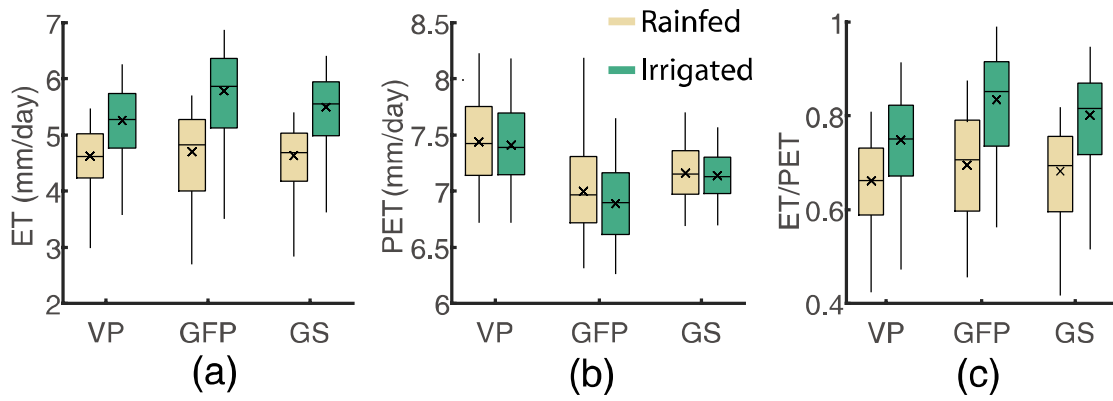
Figure 4: Boxplot of maize phenological date (a) and duration (b-c) for irrigated and rainfed maize areas. The spatial pattern of phenological date and duration differences between irrigated and rainfed maize areas (d-e).



773

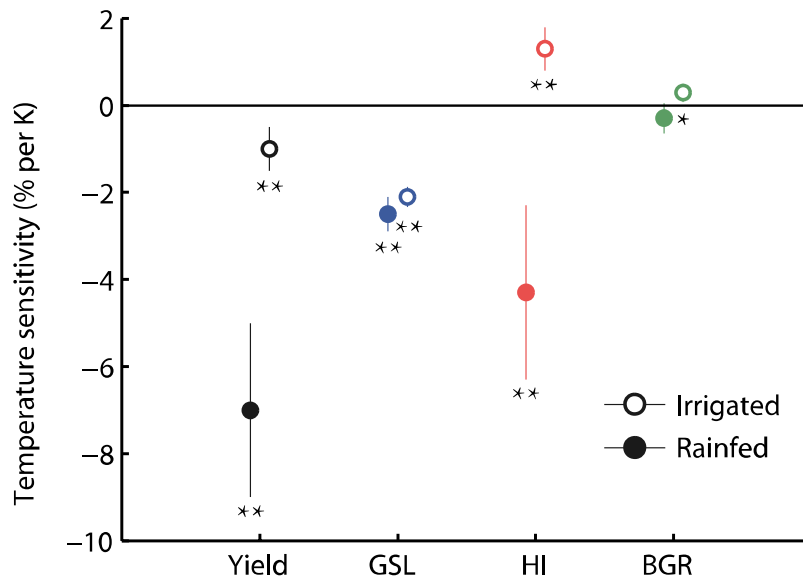
774 **Figure 5:** Boxplot of GDD and EDD estimated with MODIS LST (a-b) and surface
 775 air temperature (c-d) for irrigated and rainfed maize areas. Boxplots indicate the mean
 776 (cross), median (horizontal line), 25--75th percentile (box), and 5--95th percentile
 777 (whiskers) of corresponding variables in all year and county combinations.

778



779
 780
 781
 782
 783
 784

Figure 6: Boxplot of SSEBop ET, MODIS PET and ET/PET for irrigated and rainfed maize areas (a-c). Spatial pattern of SSEBop ET, MODIS PET and ET/PET differences between irrigated and rainfed maize areas (d-f).

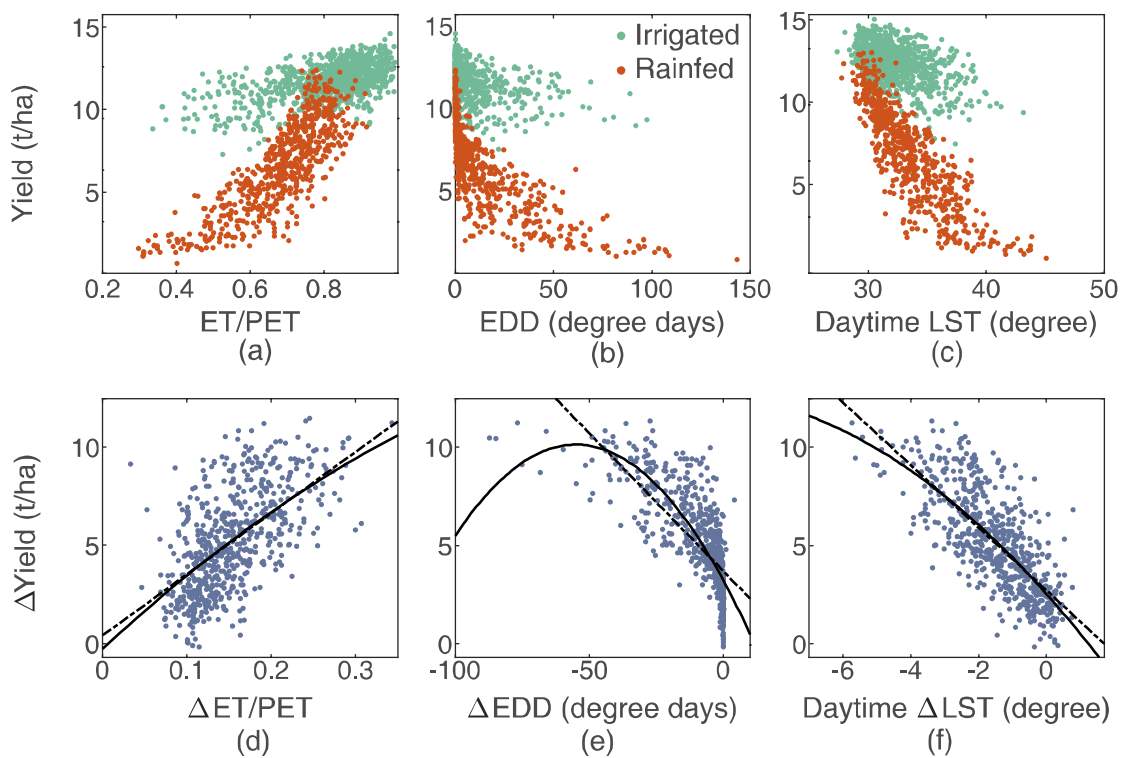


785

786 **Figure 7:** Temperature sensitivity of yield and yield components (GSL, HI and BGR)
 787 for irrigated and rainfed maize areas. The error bars represent the 95% confidence
 788 interval of estimated temperature sensitivity. ** indicates a significant estimation of
 789 temperature sensitivity with $p < 0.01$ while * indicates significance with $p < 0.05$.

790

791

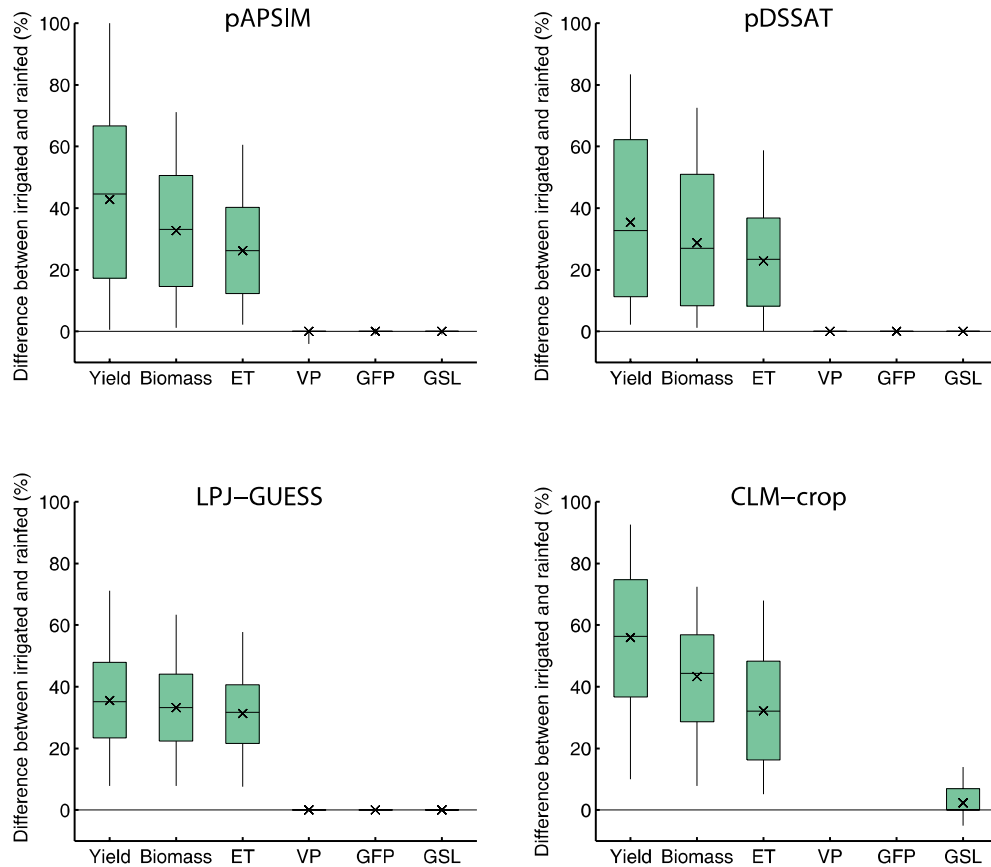


792

793 **Figure 8:** Response of maize yield to ET/PET (a), EDD (b) and daytime LST (c) in
 794 both irrigated and rainfed maize. Response of yield differences to ET/PET (d), EDD

795 (e) and daytime LST (f) differences between irrigated and rainfed maize. The linear
 796 (dash black line) and quadratic (solid black line) response curves of $\Delta Yield$ to
 797 $\Delta ET/PET$, ΔEDD and ΔLST are shown in d-f.

798
 799
 800



801

802 **Figure 9:** Boxplot of crop model simulated yield, biomass, ET and phenological
 803 duration (VP, GFP and GSL) differences between irrigated and rainfed maize areas.
 804 For phenological duration, CLM-crop only reports GSL.